Tectonophysics 642 (2015) 58–70

Contents lists available at ScienceDirect

Tectonophysics

journal homepage: www.elsevier.com/locate/tecto

Volcano-structural analysis of La Garrotxa Volcanic Field (NE Iberia): Implications for the plumbing system

Xavier Bolós [a,*], Joan Martí [a], Laura Becerril [a], Llorenç Planagumà [b], Pablo Grosse [c], Stéphanie Barde-Cabusson [a]

[a] Institute of Earth Sciences Jaume Almera, ICTJA-CSIC, Group of Volcanology, SIMGEO (UB-CSIC), Lluís Solé i Sabarís s/n, 08028 Barcelona, Spain
[b] Tosca Environmental Services, Parc Natural de la Zona Volcànica de la Garrotxa, c/Santa Coloma, 17800 Olot, Spain
[c] CONICET, Fundación Miguel Lillo, Tucumán, Argentina

ARTICLE INFO

Article history:
Received 23 May 2014
Received in revised form 29 December 2014
Accepted 31 December 2014
Available online 8 January 2015

Keywords:
Garrotxa Volcanic Field
Monogenetic volcanism
Magma ascent rate
Plumbing system
Extensional tectonics

ABSTRACT

The Garrotxa Volcanic Field is related to the Neogene–Quaternary European Rift system and is the youngest representation of monogenetic volcanism in the Iberian Peninsula. It encompasses over 50 eruptive vents, most of them well-preserved cones, in an area of about 600 km^2 lying between the cities of Olot and Girona (NE Spain). In this paper we investigate the relationship between the Neogene extensional tectonics and the spatial distribution of the volcanoes in the area. The analysis includes the distribution of faults, fissures and vents, as well as morphostructural lineaments, and the morphometrical analysis of volcanic cones and craters. In addition, we use the location of the regional seismicity recorded since 1978 and the sites of freshwater springs and mantle-derived gases as indicators of active faults and open fractures. Finally, we consider the location of ultramafic xenoliths within volcanic deposits as a way of identifying the deepest fractures in the zone and estimating magma ascent velocities. The results obtained show that this volcanic area consists of an extensional basin delimited by two principal NW–SE faults that favoured the ascent of magma from either the source region or from shallower reservoirs located at the base of the crust. Towards the upper part of the crust, magma transport was captured by shallow secondary extensional NNW–SSE striking faults whose formation is linked to the slight transtensional movement of the main bounding faults. Our study provides evidence of how the local stress field and contrasts in substrate stratigraphy could have controlled magma migration, which suggests that precise knowledge of the stress configuration, substrate geology and structural discontinuities in such regions is crucial in the forecasting of monogenetic volcanism.

1. Introduction

Basaltic monogenetic volcanic fields related to rift zones are found the world over and are expressed on the Earth's surface by alignments of pyroclastic cones and vents and parallel faults and eruptive fissures (Fiske and Jackson, 1972; Walker, 1999). A volcanic eruption marks the end of the process whereby magma rises from its source in the upper mantle to the surface (e.g. Brenna et al., 2011; McGee et al., 2011). The final geometry of the magma pathway towards the surface is directly controlled by the stress field and always tends to follow a path normal to the minimum stress (Cebrià et al., 2011; Connor and Conway, 2000; Gudmundsson and Philipp, 2006; Le Corvec et al., 2013; Rubin, 1995). In monogenetic volcanic fields the distribution and magnitude of different stress fields can be related to tectonic and gravitational forces that, in turn, are linked to (a) basement geometry, (b) local topography, (c) stress changes occurring during dyke propagation, and (d) stress barriers related to structural discontinuities and rheological changes in stratigraphic successions (Acocella and Tibaldi, 2005; Clemens and Mawer, 1992; Gretener, 1969; Gudmundsson, 2003; Gudmundsson and Philipp, 2006; Kavanagh et al., 2006; Tibaldi, 2003; Tibaldi et al., 2014). Deciphering the potential pathways that magma uses to reach the surface is of crucial importance when conducting hazard assessment in volcanic areas.

To understand the structural setting of a monogenetic volcanic field and to infer the pathways used by magma on its ascent to the Earth's surface we need to know the distribution and characteristics of its internal plumbing system. However, in recent areas this can only be achieved using indirect geophysical methods. Over the last twenty years, several geophysical studies have been devoted to the geological–structural characterisation of the feeding systems of monogenetic volcanic areas (or, more generally, of active volcanic districts) (e.g. Bibby et al., 1998; Blaikie et al., 2014; Di Maio et al., 1998, 2000; Nishi et al., 1996; Portal et al., 2013).

In La Garrotxa Volcanic Field (NE Iberia), geophysical studies of this type have been conducted in recent years and have been successful in describing the stratigraphy of the area and the shallow structure beneath the volcanic deposits (Barde-Cabusson et al., 2013, 2014; Bolós et al., 2012, 2014a, 2014b). Results have confirmed in general terms that this volcanism is mainly controlled by NW–SE faults that

* Corresponding author.
E-mail address: xavier.bolos@gmail.com (X. Bolós).

http://dx.doi.org/10.1016/j.tecto.2014.12.013
0040-1951/

also control the post-Alpine structural evolution of the area. However, the exact structural control and the role played by the major and subordinate faults in determining the distribution of vents and the frequency and size of the eruptions is not known.

In order to improve our understanding of the structural constraints of La Garrotxa volcanism, we combined the results of these geophysical studies with a new volcano-structural analysis that includes data on the distribution of faults, fissures and eruptive vents, the identification of morphostructural lineaments by remote sensing, and a DEM (Digital Elevation Model) derived morphometrical analysis of volcanic cones and craters. In addition, we took into account all the epicentres of regional seismic events recorded by the Geological Survey of Catalonia (IGC) (www.igc.cat) since 1978, as well as the distribution of CO_2-rich freshwater springs, and springs and wells with high radon levels, as an indication to active faults and open fractures, respectively. Finally, we analysed the distribution of upper mantle xenoliths and lower crust

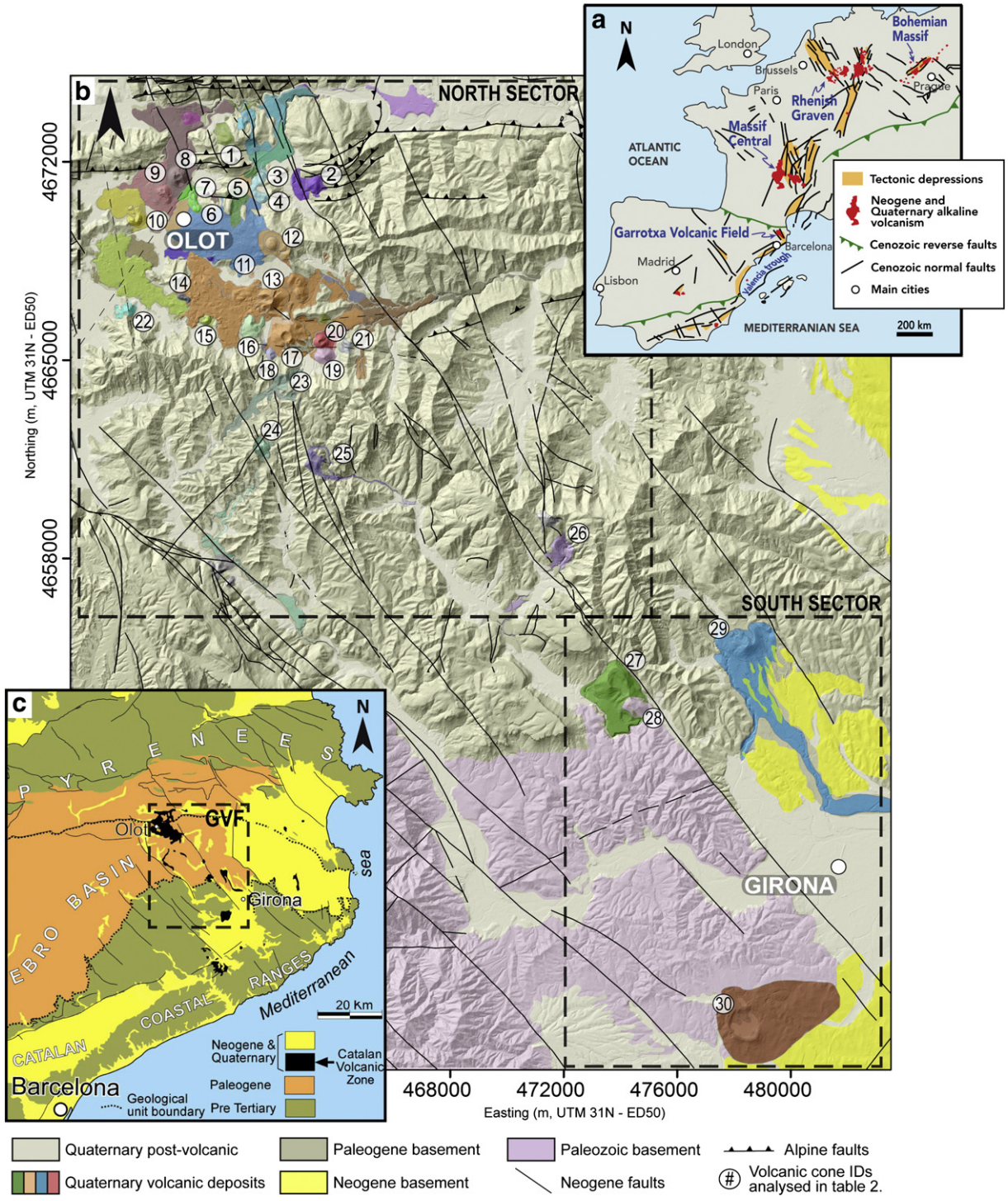

Fig. 1. Regional setting and location of the study area. a) Simplified map of the distribution of the European Cenozoic rift system. b) Volcano-stratigraphic map and structural elements of the study area (modified from Bolós et al., 2014b). Numbers correspond to the ID of the cones analysed in Table 2. Boxes locate the northern and southern sectors. c) Simplified geological map of the Catalan Volcanic Zone (modified from Guérin et al., 1985).

cumulates as an indication of the depth reached by fractures and faults, and used the largest of these xenoliths to estimate magma ascent velocities. The data obtained were combined into a conceptual model describing how magma was transported from the source to the surface in La Garrotxa Volcanic Field, which can bring some clues for such processes in other monogenetic volcanic fields.

2. Geological setting

Mafic alkaline volcanism is widely distributed along the European Cenozoic Rift System that comprises four main volcanic areas: the Rhenish Graben in Germany, the Lusatian Volcanic Field in Eastern Europe, the Massif Central in France and the Valencia Trough in Spain

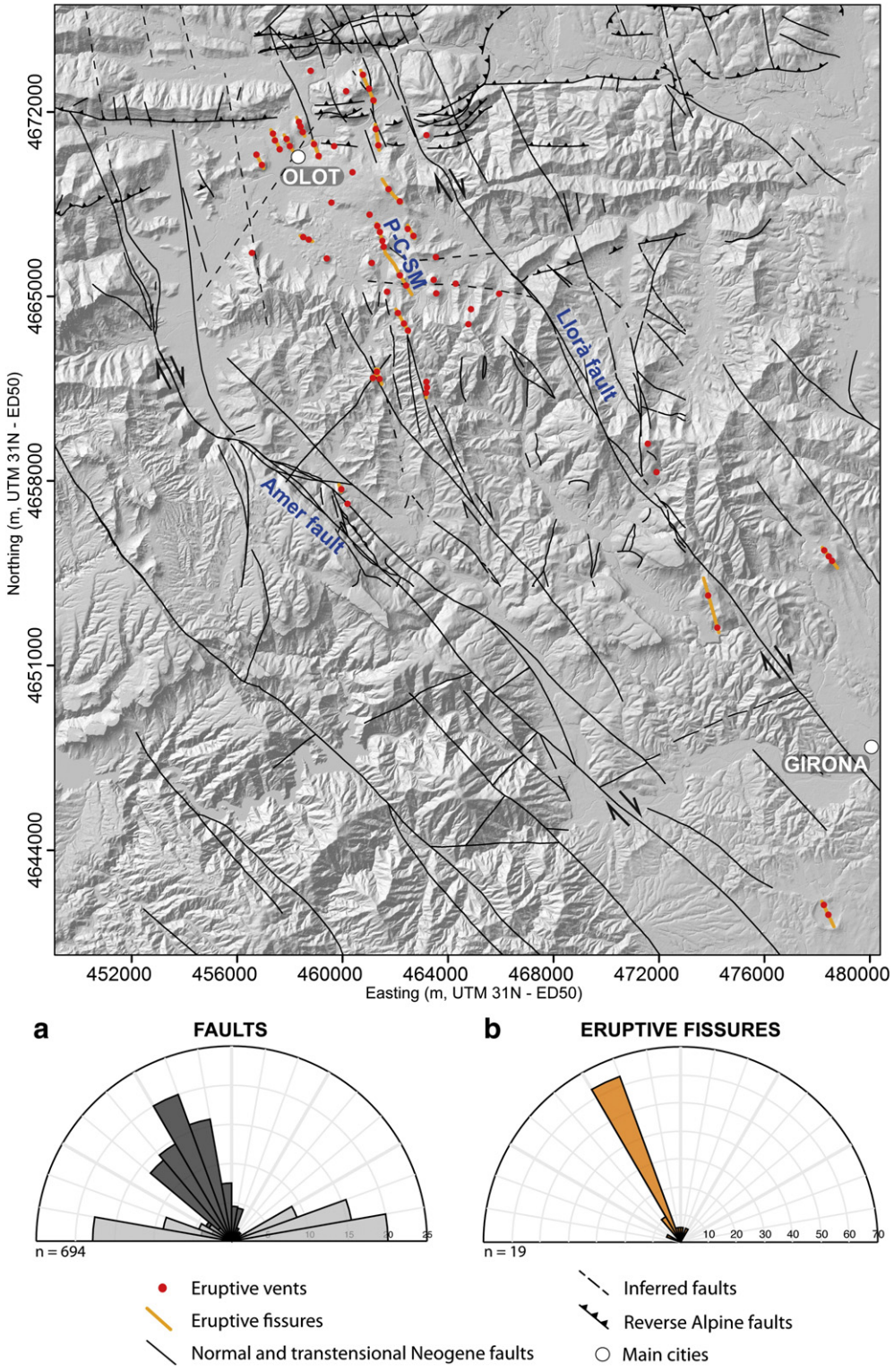

Fig. 2. Volcano-structural map of La Garrotxa Volcanic Field. a) Rose diagram of fault strike; Neogene faults are represented in dark grey and Alpine reverse faults in light grey. b) Rose diagram of the strike of eruptive fissures.

(Fig. 1a) (Dèzes et al., 2004; Downes, 2001; Michon and Merle, 2005; Ziegler, 1992). The study area is part of the Valencia Trough, a NE–SW-oriented Neogene basin lying offshore between the Iberian Peninsula and the Balearic promontory in northeastern Spain (Fig. 1a). The most important concentration of Middle Miocene-to-recent volcanism in the Valencia Trough is found in the Catalan Volcanic Zone (CVZ) in the NE Iberian Peninsula (Martí et al., 1992, 2011). This area is characterised by a series of NW-striking graben and horst structures that have controlled Neogene–Quaternary volcanism and sedimentation (Goula et al., 1999; Martí et al., 1992) (Fig. 1c).

The most recent episode in this volcanism corresponds to La Garrotxa Volcanic Field (GVF) (0.7 Ma to early Holocene) (Araña et al., 1983; Bolós et al., 2014b). This field covers an area of about 600 km^2 located between the cities of Olot and Girona (Fig. 1) and is bounded by two regional conjugated Neogene normal faults with a transtensional component (Goula et al., 1999; Olivera et al., 2003): the Amer Fault to the east and the Llorà Fault to the west (Figs. 1 and 2). These two faults are responsible for the distribution of the volcanism in the area, as well as its seismicity and the fluvial network pattern (Barde-Cabusson et al., 2014; Cimarelli et al., 2013; Martí et al., 2011; Saula et al., 1996). To the north, the volcanic field is limited by an E–W reverse fault system, out of which is not related to the subsequent magmatism. The northern sector of the area is characterised by a basement composed of Paleogene and Quaternary sediments, while the southern sector has an older basement formed not only by Paleozoic granites and schists, but also by Neogene sediments (Fig. 1b). The GVF contains over 50 eruptive vents, most of them well-preserved cones, the main concentration being located in the northern sector of the area (Fig. 1b). Volcano types include cinder and scoria cones, spatter cones, tuff rings and maars. Compositionally, they mainly correspond to basanites and alkaline basalts (Araña et al., 1983; Cebrià et al., 2000; Martí et al., 1992). Some volcanoes contain ultramafic to mafic xenoliths including pyroxenites, melanogabbros, amphibolites and spinel lherzolites, of which the pyroxenites are the most abundant (Bianchini et al., 2007; Galán et al., 2008; Llobera, 1983; Neumann et al., 1999). Pressure and temperature estimates suggest that the pyroxenites, melanogabbros and amphibolites may have crystallised in magma chambers located at the crust–mantle boundary (Neumann et al., 1999), which, according to geophysical estimates, is located at a depth of ~30 km (Fernández et al., 1990; Gallart et al., 1984, 1991); on the other hand, the spinel lherzolites may derive from the source region in the asthenospheric mantle (Bianchini et al., 2007).

3. Methodology

The present study uses the volcano-stratigraphy and the relative age of edifices and volcanic deposits described in Bolós et al. (2014b). New fieldwork and remote sensing analyses were conducted in order to identify and measure the main volcano-structural features such as vents, eruptive fissures and faults (Fig. 2). Vents were represented on our map (Fig. 2) by points corresponding to the middle of the craters of isolated cinder cones and of coalescent cinder cones with multiple craters that belong to the same eruptive fissure. Remotely-sensed structural mapping was performed in a GIS environment (ESRI© ArcGIS 10) at 1:5000 scale. We have used orthophotographs (1:2500) which have been the basis of the digitalisation, and aerial photographs (1:18,000) and Digital Elevation Models (DEM; 5- and 2-m resolution) produced by the Cartographic Institute of Catalonia (ICC; www.icc.cat) as support material. Geological maps produced by the Geological Survey of Spain and Geological Survey of Catalonia (IGC; 1:25,000; www.igc.cat; IGME; 1:50,000, http://cuarzo.igme.es/sigeco/, 2011) were also used as the basis on which to add our new information. Structural analyses included the determination and comparison of lineaments obtained from field observations, orthophotographs and different illumination-shaded relief DEMs, as well as a statistical analysis of the orientation and length of lineaments (see Table 1 of supplementary material). We also analysed the profile and direction of several streams and rivers based on a drainage network map extracted by spatial analysis of a DEM, in order to detect preferential orientations that could be related to tectonic features (Fig. 3).

Besides the identification of volcanic edifices, the eruptive vents were mapped as individual points of magma emission on the surface, which allowed us to delineate the eruptive fissures corresponding to lines connecting coeval volcanic vents, i.e. opened during the same eruption (e.g. Becerril et al., 2013; Bonali et al., 2011; Corazzato and Tibaldi, 2006; Paulsen and Wilson, 2010; Tibaldi, 1995). Fieldwork addressed to identify volcanic deposits and their stratigraphic relationships allowed us to verify the number of existing vents, as well as the lengths and strikes of eruptive fissure (Fig. 2 and Table 3 of supplementary material).

A morphometric analysis was performed on all well-preserved cones showing clear topographic expressions. We analysed a total of 30 cones and craters in the northern and southern sectors of the GVF using DEMs with resolutions of 2 and 5 m, respectively. The cone base and crater outlines were manually delimited along slope breaks and by consulting geological maps (Bolós et al., 2014b; IGC; 1:25000; www.igc.cat). Morphometric parameters of each cone and crater were extracted using the MORVOLC program (Grosse et al., 2009, 2012). MORVOLC is an IDL-language code designed specifically to compute, from a given DEM and volcano outline, a set of morphometric parameters that describe the size and shape of the volcano; for details on the code and the obtained parameters see Grosse et al. (2012). The following parameters were considered for this study: (a) Ellipticity Index (EI) of the cone base and crater outlines; EI is a measure of elongation equal to:

$$EI = \left(\pi * (L/2)\text{^}2\right)/A \quad (1)$$

where L is the length of the maximum/major outline axis and A is the outline area), (b) the average EI of all the all elevation contours (5 m contour interval) above the cone base, (c) the major axis azimuths of cone and crater outlines, (d) the circular average azimuth of the major axes of all the elevation contours above the cone base, and (e) the azimuth and direction of crater breaching, where present.

No dyke outcrops have been found in the studied area, probably due to its recent age and lack of significant erosion. However, several feeder dykes hidden by their own deposits were identified using Electric Resistivity Tomography (Bolós et al., 2012, 2014a). Using the geological information of Bolós et al. (2014b), we have carried out new structural interpretations of the geological maps and mapped faults of IGC and IGME. Preferential orientations that may follow main structural trends were also obtained from the drainage network map extracted by spatial analysis of a DEM. Rose diagrams of fissures, faults and drainage networks were produced and analysed. We also took into account the distribution of the main freshwater springs existing in the study area (Fig. 4) to indicate the presence of open fractures and faults. We digitized and georeferenced a total of 191 springs shown on the topographic maps of the Catalan Geographic Institute (www.icc.cat), along with others identified during fieldwork, for a total of 254 springs. High concentration of endogenous gases (i.e. radon, CO_2) in freshwater springs is assumed to indicate the presence of deep fractures with high permeability values (Kresic, 2010; Wattananikorn et al., 1998). In the studied area the highest values of endogenous gases, including 12 measurements of CO_2 in freshwater springs and 53 groundwater radon measurements in water wells and springs, were found in correspondence with active Quaternary faults (Moreno et al., 2014; Zarroca et al., 2012) (Fig. 4).

The location, depth and magnitude of seismic events were also incorporated into our dataset (Fig. 5). Although seismic events are not that abundant in the northeastern part of the Iberian Peninsula, it was possible to collect accurate data regarding the earthquakes recorded since 1978 by the Geological Survey of Catalonia (www.igc.cat) (Table 4 of supplementary material). We compiled the location, depth and magnitude of the seismic events; locations of seismic events were

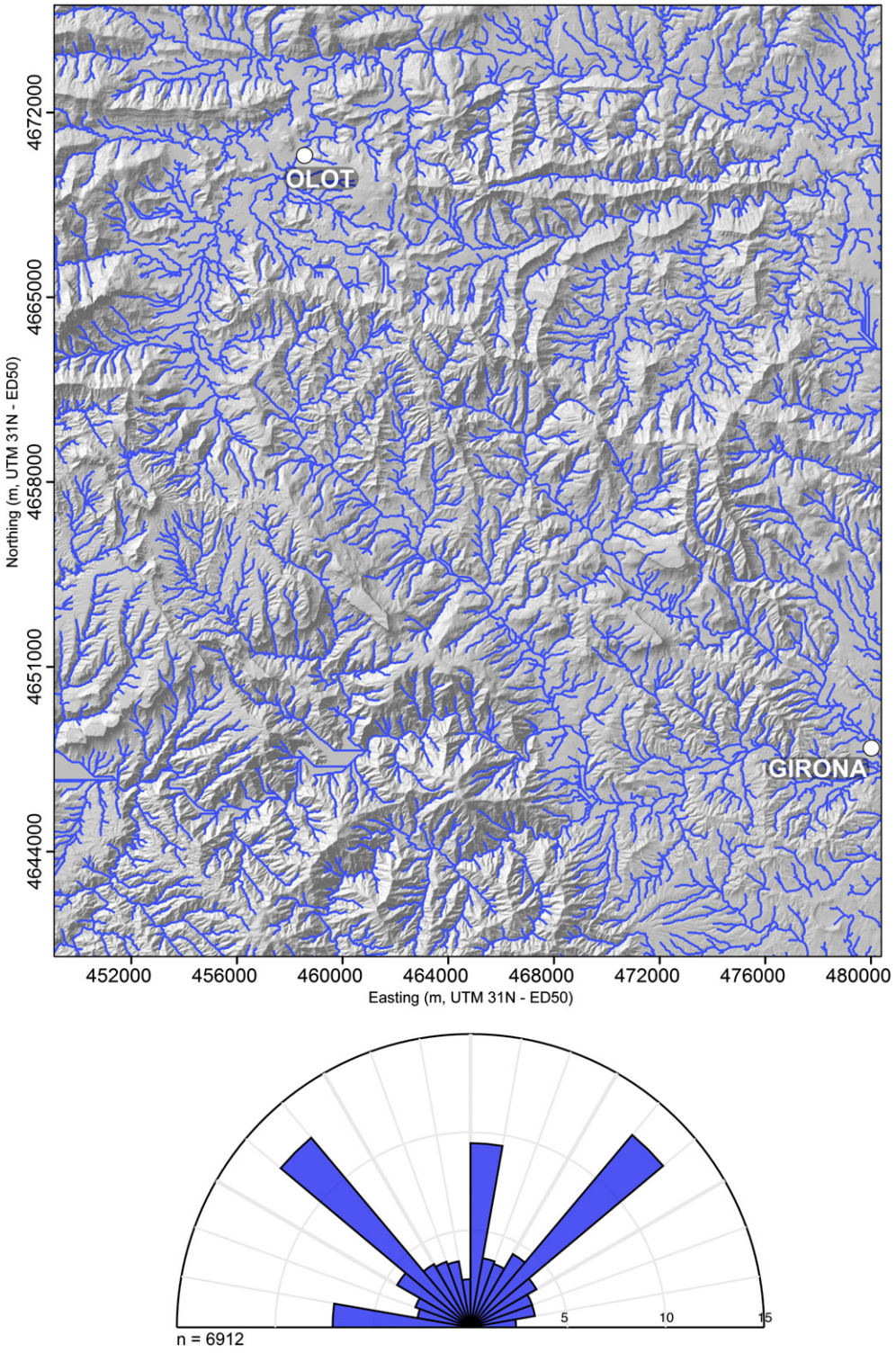

Fig. 3. Drainage network of La Garrotxa Volcanic Field. Trends are represented in a rose diagram.

represented on the structural map. The average distance between seismic stations is 30 km and data pertaining to earthquakes located within this network have an accuracy of 2–3 km for epicentres and 5 km for depths (Goula et al., 1999).

The presence of upper-mantle and lower-crust xenoliths in volcanic products has been used as an indicator of the depth of magma pathways and to estimate magma ascent velocities (Jankovics et al., 2013; Klugel, 1998; Mattsson, 2012; Sachs and Stange, 1993; Spera, 1984; Sparks et al., 1977, 2006; Tsuchiyama, 1986). In this study we mapped the distribution of the volcanoes containing lower-crust xenoliths, mantle-derived xenoliths or both types (Fig. 6), as a way of estimating the depth of the fractures and faults through which magma is transported to the surface. Calculations of magma ascent velocities were made on the basis of the assumption that magma (melt) was – in rheological and petrological terms – similar throughout the study area (i.e. basalts and basanites) (Araña et al., 1983; Cebrià et al., 2000; Martí et al.,

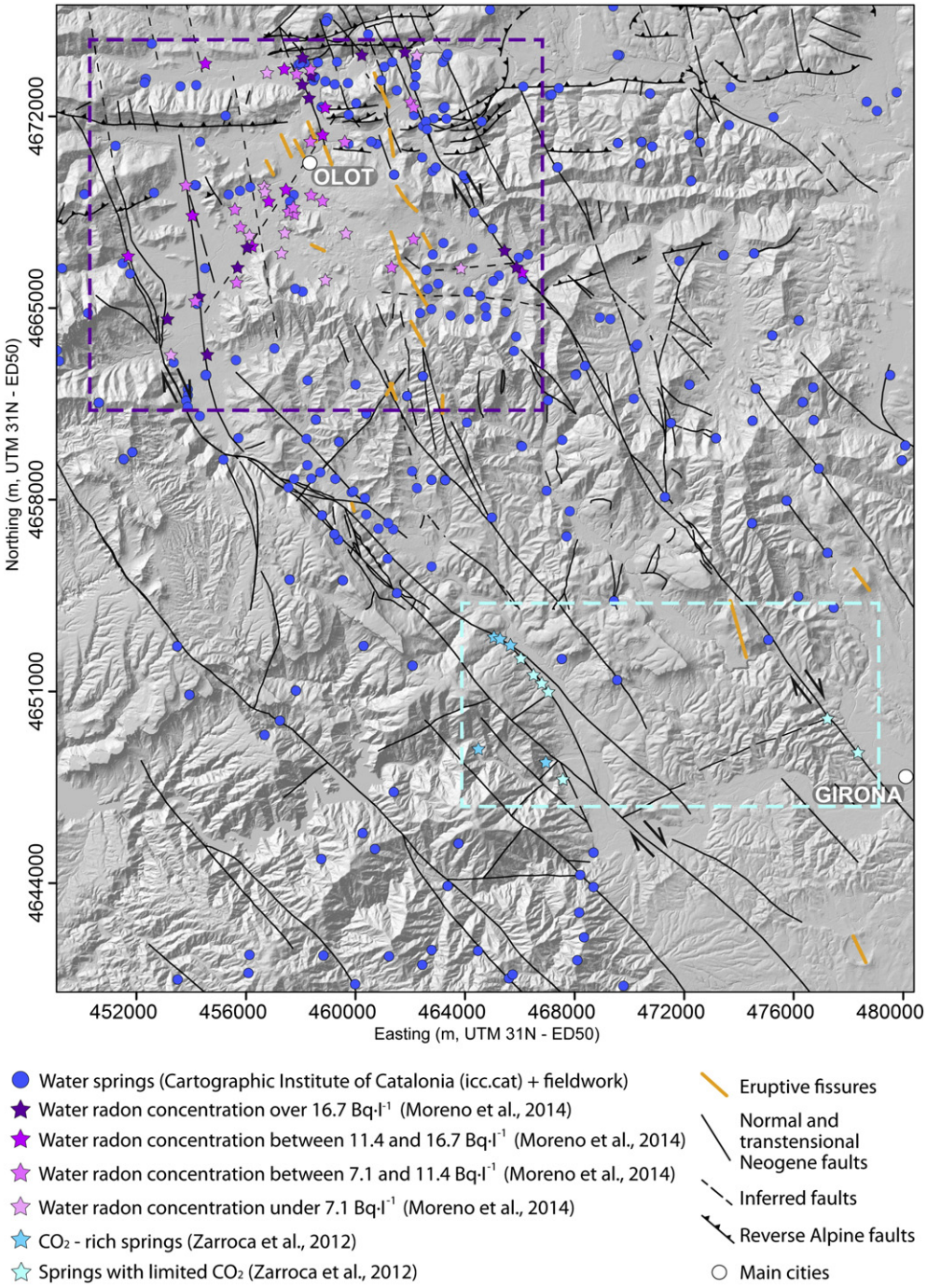

Fig. 4. Map of freshwater springs (blue dots) and water radon concentrations (purple stars) obtained by Moreno et al. (2014), and CO_2-rich springs (blue stars) obtained by Zarroca et al. (2012). Structural elements as in Fig. 2.

1992), although the distribution of xenoliths does in fact vary. In addition, we assumed that during its ascent the magma did not undergo any significant temperature variation, as has been suggested by Cimarelli et al. (2012), and that its rheology was close to that of a Newtonian fluid, as should occur in the case of a magma of this composition with a crystal content of less than 15% (see Vona et al., 2011). With these assumptions in mind, we applied the method of Spera (1980, 1984), which defines:

$$Re_n = \rho D_n u_n / \eta_l \tag{2}$$

$$u_n = \left((8R_n \Delta\rho g)/\left(3C_{dpl}\right)\right)^{1/2} \tag{3}$$

where η_l, u_n, R_n, $\Delta\rho$, ρ_l, g and C_d represent the Newtonian viscosity, nodule settling velocity, radius, density difference between melt and xenolith, density of melt, gravity value, and drag coefficient, respectively. C_d is related to the nodule settling velocity and hence to Re_n. For our samples we considered $Re_n > 0.1$ assuming that this magma is very fluid and that some of the xenoliths found are of large size (up to 80 cm across), and therefore we applied:

$$C_d = 18\,Re_n^{-3/5}. \tag{4}$$

In order to estimate the minimum ascent rate we took into account the maximum size of xenoliths found in the area. The density of the melt was measured from natural rock glass by remelting a representative

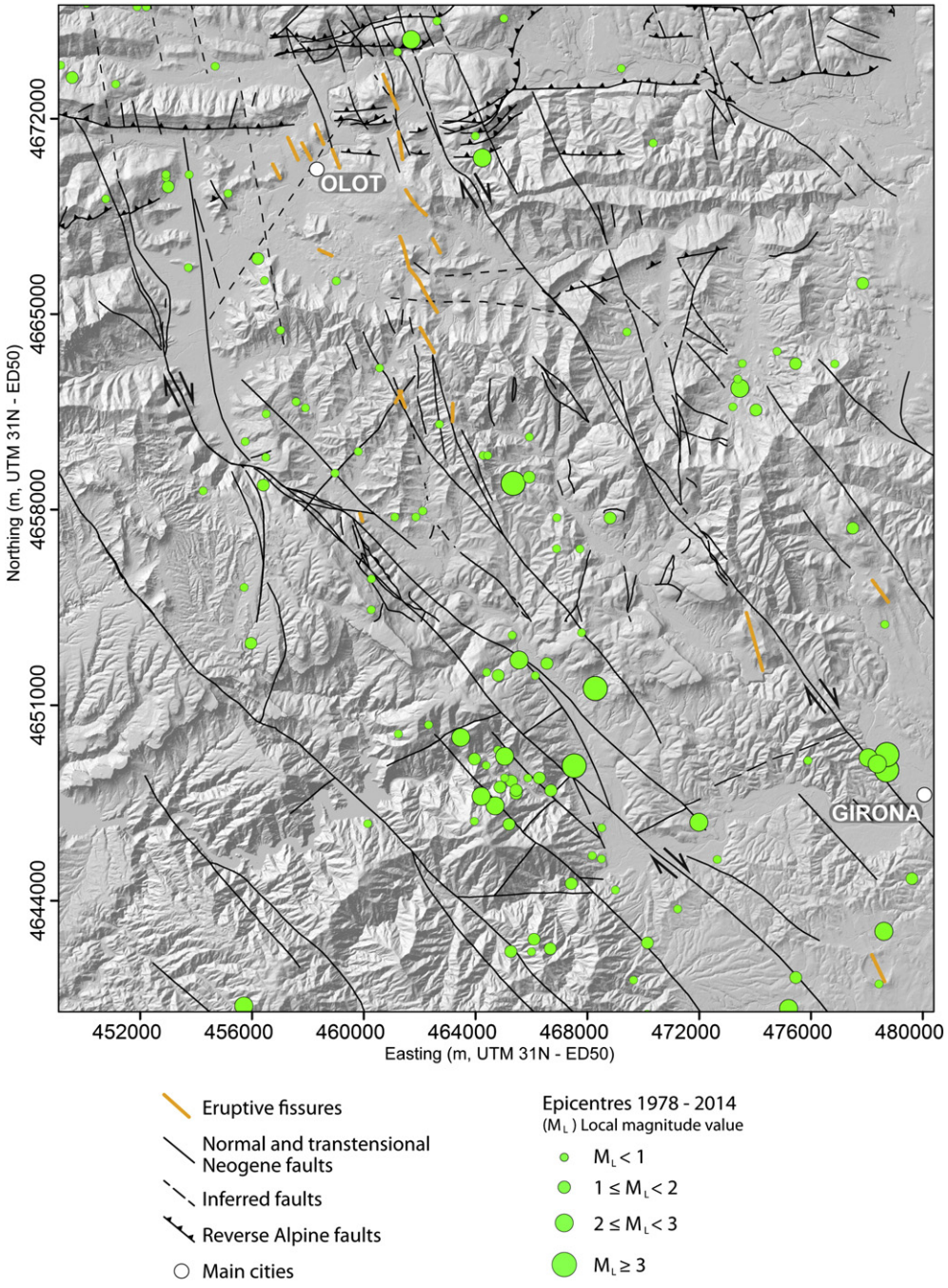

Fig. 5. Epicentral map of regional seismic events recorded by the Geological Survey of Catalonia (IGC) since 1978 (Table 4, supplementary material), with indication of local magnitude (M_L). Structural elements as in Fig. 2.

sample in a Pt crucible at 1400 °C for 5 h in an open atmosphere to remove vesiculation. The density obtained was 2.53 g/cm^3. Finally, we used the method of Vona et al. (2011) to estimate the viscosity (40 to 50 Pa·s).

4. Results

Although the GVF is constrained mainly between two Neogene faults, the Amer and Llorà faults, there are a few other volcanic outcrops and vents located outside these structural limits, mainly east of the Llorà fault (Fig. 2). No vents are directly located on the Amer and Llorà faults. All the vents identified in this study are located on subordinated faults. In the field it is clear that the majority of volcanic deposits have not been affected by the Neogene faults (Bolós et al., 2014b). Only the main Amer fault affects deposits from two volcanoes but not their vents (Fig. 1b). Most of the volcanic deposits located in the north of the study area cover basement rocks, preventing identification of subordinate faults. Towards the north, a set of E–W reverse faults and thrusts formed during the Alpine Orogeny delimits the volcanic field, but it is intersected by the same NW–SW Neogene fault system that constrains the volcanic field further to the south (Fig. 2). The maximum length of the main Neogene faults is ~43 km, while the maximum length of the secondary faults is ~7 km (Table 1 of supplementary material).

A total of 67 eruptive vents were mapped in the study area. The majority of eruptive vents (83.5%) is located in the northern sector of the GVF, around the city of Olot, while only a few vents (16.5%) are located in the southern sector (Fig. 2) (Table 1 of supplementary material). However, the volcanoes in the southern sector are larger and have

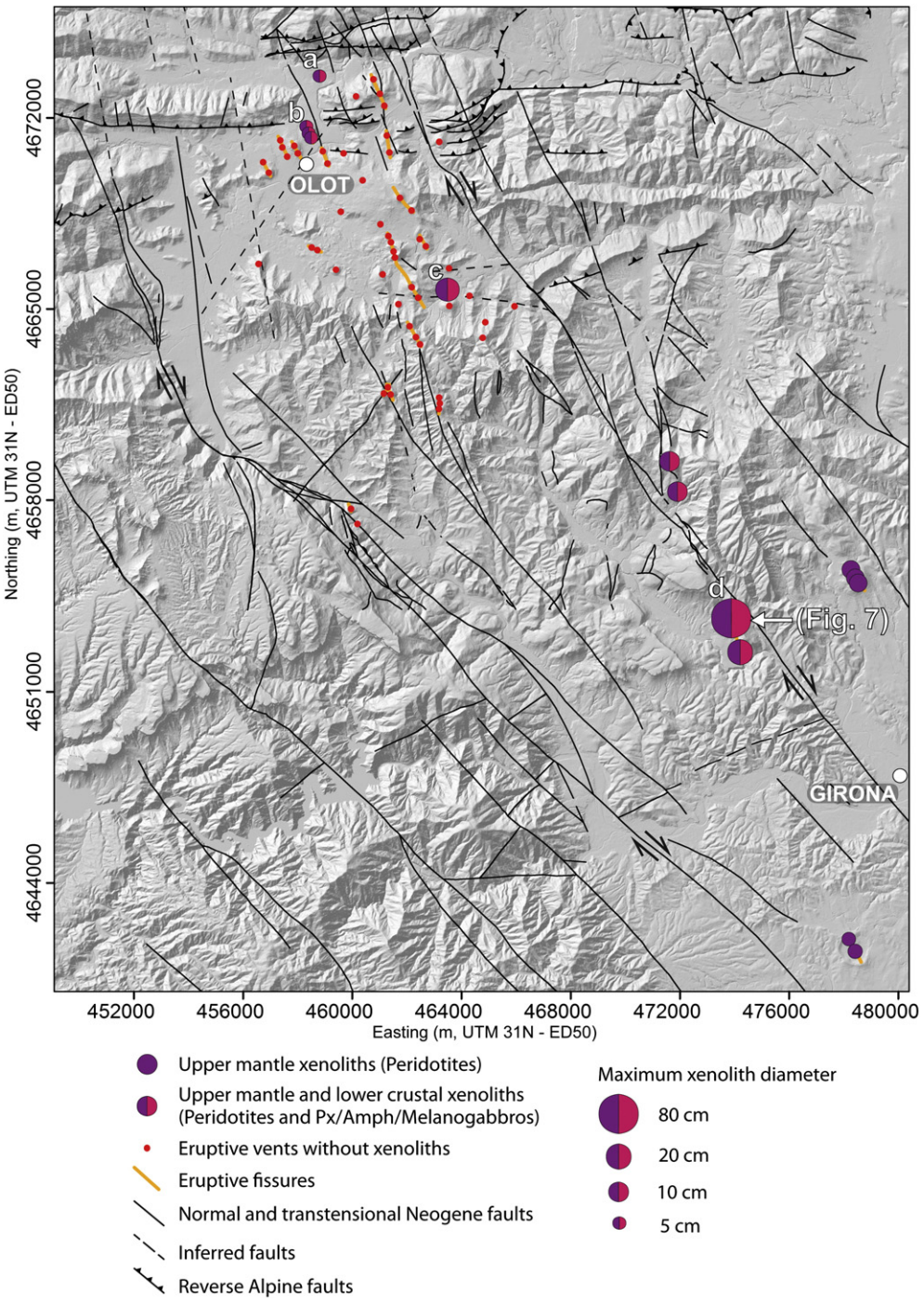

Fig. 6. Structural map with overimposed distribution of all ultramafic xenoliths (upper-mantle and lower-crust xenoliths) found in the study area, with an indication of their maximum size. a: La Canya; b: La Garrinada; c: Rocanegra; d: Puig de la Banya del Boc.

emitted more magma than those in the northern sector (Bolós et al., 2014a). Several volcanic deposits that cannot be associated with any eruptive vent, either because they have been eroded or covered by more recent volcanic materials, have not been considered in our structural analysis.

The coeval alignments defined by 44 of the eruptive vents allowed us to infer 18 eruptive fissures (Fig. 2). All fissures except one have a similar trend, with an average strike of ~N155°E. The Pomareda–Croscat–Santa Margarida eruptive fissure, located in the central area of the northern sector (P-C-SM in Fig. 2) is the longest one, measuring ~3050 m, and was recognized through geological fieldwork and geophysical studies (Barde-Cabusson et al., 2013, 2014). The shortest fissure measures 287 m (Table 1 of supplementary material), the average fissure length is 968 m and most of the fissures measure between 400 and 1200 m (Table 3 of supplementary material).

About two thirds of the total of 30 analysed cones stand on relatively flat bases (basal dip < 8°) and have quite symmetric flanks, whereas the other third are built on steeper and irregular topography and thus have uneven flanks. The cones have average basal widths (diameter of area-equivalent circle) between 160 and 1430 m (average 610 m) and heights between 22 and 169 m (average 73 m). 27 of the 30 cones have visible craters, with some cones having 2 or 3 coalescing craters (i.e. multiple craters). Of a total of 36 analysed craters, 21 are breached. Closed craters have average widths between 41 and 391 m (average

220 m; excluding one large crater with a width of 1160 m, corresponding to the maar-diatreme phase of Crosa de Sant Dalmai volcano) and depths between 5 and 60 m (average 20 m). The EI of the cone bases vary between 1.2 and 2.1, and for the closed crater outlines between 1.2 and 1.5; average EI calculated for all elevation contours vary between 1.3 and 4.9. Elongation azimuths of the cone bases, closed crater outlines, multiple crater outlines and elevation contours define two orientation trends: a main NW–SE to NNW–SSE trend and a secondary NE–SW to ENE–WSW trend. Although breaching direction cannot be considered as a good indicator of fissure strike as it can be controlled by several factors (Corazzato and Tibaldi, 2006; Tibaldi, 1995), the breached craters have orientations similar to that of the elongation parameters, with breaching mainly towards the NW and NNW (i.e. parallel to the main orientation trend) and subordinately towards the NE (i.e. parallel to the secondary trend) (see Table 2 in supplementary material).

The analysis of the drainage network also allowed us to distinguish different trends that support the main structural features of the area; the four principal stream directions identified were NW–SE, NE–SW, N–S and E–W (Fig. 3).

The majority of freshwater springs identified and plotted on the structural map coincide with the main tectonic elements such as Neogene faults and the Alpine reverse faults (Fig. 4). However, a few springs are not associated to any structural element. Moreno et al. (2014) analysed the endogenous gas content of springs and water wells in the northern part of the study area. A total of 41 measurements of water radon concentration with values between 16.7 and 7.1 $Bq \cdot l^{-1}$ were made, with most located on the Amer and Llorà faults and others on other Neogene secondary faults (Fig. 4). Furthermore, Zarroca et al. (2012) measured a total of 12 CO_2-rich springs located in the southern part of our study area on the central part of the Amer fault (Fig. 4). The emissions of CO_2 in this area are clearly measurable in the field as sustained bubbling in freshwater springs.

A total of 201 seismic events have been recorded in the GVF since 1978 (Fig. 5) and are mostly distributed along the Neogene faults clustered between the Amer and Llorà faults. Moreover, there is a greater density of seismic events in the central part of the Amer fault that coincides with high CO_2 emissions. The maximum earthquake magnitude recorded in this period was M_L 3.5 in 1983 on the Amer fault (Fig. 5) (Table 4 of supplementary material). Despite the low present-day seismicity, a swarm of powerful earthquakes that took place in 1427–1428 with intensities in the area ranging between VI and VIII (Mercalli scale) has been attributed to a movement of the Amer fault (Fontserè and Iglésies, 1971; Goula et al., 1999; Olivera et al., 2003, 2006; Perea, 2009; Zarroca et al., 2012).

As explained above, we also considered the distribution of mantle-derived xenolith and crustal cumulates as a way of indicating the depth of the faults and fissures through which they were transported to the surface, and of estimating magma ascent velocities. The distribution of all ultramafic xenoliths found in the area along with their maximum sizes is shown in Fig. 6. We observed that the presence of xenoliths is related to the volcanoes located near – but not on – the main Llorà fault. In the area with the greatest density of volcanic cones (northern area) (Fig. 1b), only three volcanoes (Rocanegra, La Garrinada and La Canya; see Fig. 6) have ultramafic xenoliths, while in the southern sector all the volcanoes have this type of xenoliths. Moreover, we observed that the presence of upper-mantle cumulates (i.e. spinel lherzolites) coincides with the volcanoes that have xenoliths, whereas the presence of lower-crust cumulates (i.e. Pyroxenites/Amphibolites) is restricted to volcanoes located in the northern sector and just one volcano in the south sector (Puig de la Banya del Boc (#27); see Fig. 6). The maximum sizes of the ultramafic xenoliths found in the GVF correspond to pyroxenites, with diameters of up to 80 cm (Fig. 7). However, most xenoliths range in size from a few centimetres to 20 cm in diameter, for both mantle-derived nodules and lower-crust cumulates. Velocities of 0.19 to 0.21 m/s have been obtained using Eqs. (2), (3), and (4), assuming a Newtonian viscosity of 40–50 Pa·s, the largest xenolith encountered (80 cm), a melt density of 2.53 g/cm^3, a xenolith density of 3.55 g/cm^3, and a gravity value of 9.8 m/s^2. The velocities obtained are in agreement with those suggested for other monogenetic volcanic fields (Harangi et al., 2013; Jankovics et al., 2013; Klugel, 1998; Mattsson, 2012; Sparks et al., 2006; Szabó and Bodnar, 1996).

Fig. 7. Photograph of the largest xenolith (pyroxenite) found in the study area (Banya del Boc volcano, southern sector of the GVF, location in Fig. 6).

5. Discussion and conclusions

The structural data presented above reveal that the evolution of the GVF has been mostly controlled by two major Neogene faults, the Amer and Llorà faults. They are both oriented NW–SE as are most of the major post-Alpine extensional faults that have defined a horst and graben structural pattern in NE Iberia. However, most of the eruptive fissures and secondary structural lineaments identified in this study show a NNW–SSE trend that runs slightly obliquely to the main faults.

The pattern shown by the eruptive fissures and subordinated structural lineaments is compatible with a slight dextral transtensional component in the two main faults (Amer and Llorà faults), as suggested by previous studies (Goula et al., 1999; Olivera et al., 2003) and indicates that magma ascent in the uppermost crust and subsequent eruptions were controlled by these subordinated fissures (Fig. 8). This structural configuration would have favoured the opening of these fractures and the transport of magma through them, at least in the final pre-eruptive stages. A similar behaviour has been described in other volcanic zones (e.g. Karakhanian et al., 2002). However, it is not clear how deep these fractures are nor what exactly was their role in transporting magma from deeper levels.

Cones and craters are elongated mainly NW–SE to NNW–SSE, subparallel to the trend defined by the fissures and faults, possibly reflecting the geometry of the magma-feeding fractures (Corazzato and Tibaldi, 2006; Tibaldi, 1995). A secondary group of cones and craters are elongated NE–SW to ENE–WSW, i.e. sub-perpendicular to the main structural trend. Considering a dextral transtensional setting, the main NNW–SSE orientation coincides with that of synthetic shears, whereas the secondary NE–SW orientation coincides with that of antithetic shears.

The presence of mantle-derived xenoliths and lower-crust cumulates suggests that the magmas that erupted in the GVF came either directly from the source region in the upper mantle or from intermediate reservoirs located at the base of the crust (Fig. 8). No evidence exists for the presence of shallower reservoirs under this volcanic field. This is also confirmed by existing petrological and geochemical data (Cebrià et al., 2000; Martí et al., 1992; Neumann et al., 1999). Therefore, what remains to be discerned is how deep the structures observed at the surface extend, and how they were used by magma to reach the surface. It is worth noting that most of the area's freshwater springs are associated with relatively shallow stratigraphic or structural discontinuities,

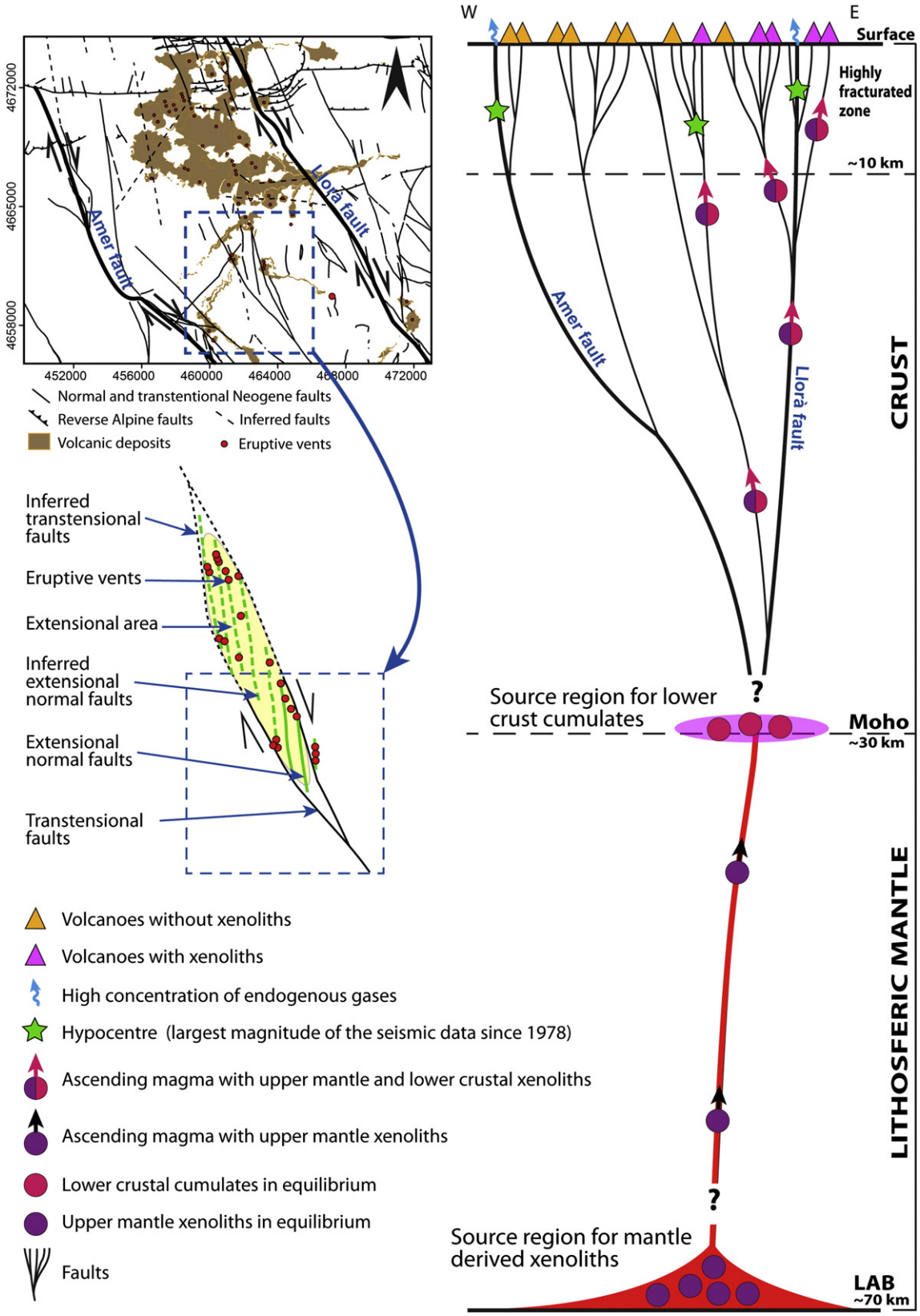

Fig. 8. Schematic representation of the relationships between regional/local tectonic faulting and the plumbing system of La Garrotxa Volcanic Field. (Right) Cross section (depth not to scale). (Left) Map view of the northern sector. LAB (Lithosphere–Asthenosphere Boundary).

while the presence of high radon and CO_2 concentrations mainly occurs along the major Neogene faults (Moreno et al., 2014; Zarroca et al., 2012), thereby indicating that the deep circulation of these mantle-derived gases is permitted through these faults (Zarroca et al., 2012). Likewise, the recorded seismicity also reveals that Neogene faults have been active recently, mainly along the Amer fault. Finally, the obtained

magma ascent rates indicate that only a relatively short time was required for magma to reach the surface, thereby suggesting the existence of preferential pathways for magma when ascending from source or accumulation regions to the eruption sites.

Taking into account all this evidence, we speculate that the Llorà fault played the most important role in driving magma from the source region, either to the base of the crust where magma occasionally accumulated (i.e. underplating) or directly to much shallower levels where it was captured by the subordinated fractures that allowed it to erupt. As indicated by the presence of lower-crust cumulates and the location of vents and eruptive fissures, the extraction of magma from the lower crust reservoir(s) was mainly controlled by the Llorà fault and, to a lesser extent, by the Amer fault, which would have acted as a conjugate major fault reaching down the base of the crust. Shallow subordinate fractures to the Amer fault would have also captured the ascending magma in its last stages and have controlled its eruption to the surface (Fig. 8).

Confirming the proposed model would require the undertaking of a detailed petrological study, which is beyond the purpose of this paper. However, the fact that mantle-derived xenoliths and the largest lower-crust cumulates are restricted to the vents related to the Llorà fault is a strong support for this model. Likewise, the volcanoes associated with this fault have the largest erupted volumes (Bolós et al., 2014b) of all volcanoes in this volcanic field, which also suggests that the Llorà fault was the main magma pathway.

The reason why magma eruptions have occurred through different NNW–SSE eruptive fissures during the history of the GVF – despite its constant and common feeding system at depth – seems to be related to the role played by these subordinate shallow fractures. They captured magma during the final stages of its ascent to the surface and so determined the point of each eruption. The shallow character of these fractures suggests that the local stress field, which was mostly controlled by the movement of the two main (Llorà and Amer) faults, did not contribute to control deeper magma migration. Under these circumstances, these shallow fractures could be easily sealed by residual magma that solidified within and it was easier for a new eruptive episode to open a fresh fracture than to reuse a previously sealed one. The sealing of these eruptive fissures by intruding magma would also obstruct the circulation of endogenous gases, as shown in the northern sector around Olot, where most eruptive vents have no associated volcanic gas emissions. This would also suggest – in accordance with the intermittent character of this volcanism (Martí et al., 1992) – that each eruptive episode corresponds to an intermittent reactivation of the main fault system every 5000–20,000 years (Bolós et al., 2014b; Martí et al., 1992). These tectonic reactivations would permit the ascent of deep magma and the opening of subordinate fractures in the uppermost crust, which would erupt each time in a different location in the volcanic field. Volcanism in the GVF is mainly concentrated in its northern sector, which suggests that the basin in this area is larger, where the accumulation of post-Alpine sediments is thicker. Moreover, the difference in basement lithology between the northern (Tertiary and Quaternary sediments) and southern (Palaeozoic granites and schists) sectors of the volcanic field may also have played a significant role in controlling the capability for magma to find pathways to reach the surface. The fact that there is no magmatism north of the GVF may be due to the important increase in thickness of the crust due to the Alpine Orogeny.

Although the GVF is the best-preserved area in the Catalan Volcanic Zone, it is not the only one containing important volumes of volcanic rocks. Older zones such as the Empordà or La Selva (Araña et al., 1983; Martí et al., 1992) also have numerous volcanic features that can be observed at the surface (highly eroded outcrops) or in the subsoil in seismic profiles and gravity and aeromagnetic maps (Casas et al., 1986; Zeyen and Banda, 1988). The tectonic evolution of the area has been controlled by a similar system of Neogene NW–SE-oriented faults, which seems to have evolved over time from NE to SW. We believe that a similar model to the one proposed in this study for the GVF could be applied to other areas in the Catalan Volcanic Zone.

In conclusion, the GVF provides a good example of the structural complexity that governs monogenetic volcanism. Although magma ascent from depth has always been controlled by the same Neogene extensional fault system that reaches the base of the lithosphere, magma transport in the uppermost crust and the eruptions were controlled by subordinate fractures originating in response to the transtensional component of the main faults. These shallow fractures were sealed by the remaining magma after each eruption and so new fractures had to be opened in each new eruptive episode, probably in association with a sporadic reactivation of the main faults. The model proposed has important implications for hazard assessment as this pattern of magma flow makes this type of volcanism largely unpredictable in terms of eruption location since the exact position of new vents does not necessarily follow a statistically pre-defined law. Any point located in the area affected by the tectonic stresses constrained by the two main faults could host a new vent if no major basement rheological contrasts exist. Moreover, the calculated ascent velocities imply that magma may travel either from the source region in the mantle or from the base of the crust to the surface in just a few days (about 40 or 17) as it has been proposed in other monogenetic fields. It is likely that most of this journey occurred aseismically due to the relatively large dimensions of the path provided by the main faults and the absence of shear movement between the fault planes, as occurred in the 2011–2012 El Hierro eruption (Martí et al., 2013). Only when magma had to open the shallow subordinate fractures did the hydraulic fracturing cause any shallow seismicity that could warn of the imminence of the eruption. Therefore, precise knowledge of the stress configuration and distribution of rheological contrasts and structural discontinuities in monogenetic fields is crucial when attempting to forecast monogenetic volcanism.

The model we have applied refers to the zone included between the two main faults of the area, the Llorà and Amer faults. However this situation is repeated outside this area where a few volcanic vents and other transtensional faults are also located. These faults have the same orientation and movement than the Llorà and Amer faults and have also associated NNW–SSE subordinated faults that have controlled some volcanic episodes (e.g.: Puig de Granollers #26 and Puig d'Àdri #29 volcanoes) (Fig. 1). These fault systems, including the Llorà and Amer faults and the adjacent major transtensional faults, resulted from the Neogene–Quaternary extensional tectonics that created the horst and graben structure of the whole CVZ. The model described for the central part of the CVZ also applies to these other adjacent sectors, and could also explain the older volcanism of the CVZ.

Supplementary data to this article can be found online at http://dx.doi.org/10.1016/j.tecto.2014.12.013.

Acknowledgements

This study was partially funded by the European Commission (FP7 Theme: ENV.2011.1.3.3-1; Grant 282759: "VUELCO") and Beca Ciutat d'Olot en Ciències Naturals. We are grateful to La Garrotxa Volcanic Zone Natural Park for their support throughout this study. We would like to thank Emilio Casciello, Núria Bagués, Joan Andujar, Pierangelo Romano, Dario Pedrazzi, Daniele Giordano, Jorge Pedro Galve, Xavier Castelltort and Daniel Nadal for their suggestions during this research. We also thank Enric Vinyals for providing us with unpublished information on seismic studies in the study area. We thank Claudia Corazzato and one anonymous referee for their thorough and constructive reviews. The English text was corrected by Michael Lockwood. Rose diagrams were obtained with the software Stereonet 8.8.4 (Cardozo and Allmendinger, 2013).

References

Acocella, V., Tibaldi, A., 2005. Dike propagation driven by volcano collapse: a general model tested at Stromboli, Italy. Geophys. Res. Lett. 32.

Araña, V., Aparicio, A., Martin Escorza, C., Garcia Cacho, L., Ortiz, R., Vaquer, R., Barberi, F., Ferrara, G., Albert, J., Gassiot, X., 1983. Neogene–Quaternary volcanism of Catalunya: structural, petrological, and geodynamic characteristics. Acta Geol. Hisp. 18, 1–17.

Barde-Cabusson, S., Bolós, X., Pedrazzi, D., Lovera, R., Serra, G., Martí, J., Casas, A., 2013. Electrical resistivity tomography revealing the internal structure of monogenetic volcanoes. Geophys. Res. Lett. 40, 2544–2549.

Barde-Cabusson, S., Gottsman, J., Martí, J., Bolós, X., Camacho, A.G., Geyer, A., Planagumà, L., Ronchin, E., Sanchez, A., 2014. Structural control of monogenetic volcanism in the Garrotxa volcanic field (Northeastern Spain) from gravity and self-potential measurements. Bull. Volcanol. 76, 788.

Becerril, L., Cappello, A., Galindo, I., Neri, M., Del Negro, C., 2013. Spatial probability distribution of future volcanic eruptions at El Hierro Island (Canary Islands, Spain). J. Volcanol. Geotherm. Res. 257, 21–30.

Bianchini, G., Beccaluva, L., Bonadiman, C., Nowell, G., Pearson, G., Siena, F., Wilson, M., 2007. Evidence of diverse depletion and metasomatic events in harzburgite–lherzolite mantle xenoliths from the Iberian plate (Olot, NE Spain): implications for lithosphere accretionary processes. Lithos 94, 25–45.

Bibby, H.M., Caldwell, T.G., Risk, G.F., 1998. Electrical resistivity image of the upper crust within the Taupo Volcanic Zone, New Zealand. J. Geophys. Res. 103, 9665–9680.

Blaikie, T.N., Ailleres, L., Betts, P.G., Cas, R.A.F., 2014. A geophysical comparison of the diatremes of simple and complex maar volcanoes, Newer Volcanics Province, south-eastern Australia. J. Volcanol. Geotherm. Res. 276, 64–81.

Bolós, X., Barde-Cabusson, S., Pedrazzi, D., Martí, J., Casas, A., Himi, M., Lovera, R., 2012. Investigation of the inner structure of La Crosa de Sant Dalmai maar (Catalan Volcanic Zone, Spain). J. Volcanol. Geotherm. Res. 247–248, 37–48.

Bolós, X., Barde-Cabusson, S., Pedrazzi, D., Martí, J., Casas, A., Lovera, R., Nadal-Sala, D., 2014a. Geophysical exploration on the subsurface geology of La Garrotxa monogenetic volcanic field (NE Iberian Peninsula). Int. J. Earth Sci. (Geol. Rundsch.) 1–15.

Bolós, X., Planagumà, L., Martí, J., 2014b. Volcanic stratigraphy of the Quaternary La Garrotxa Volcanic Field (north-east Iberian Peninsula). J. Quat. Sci. 29 (6), 547–560.

Bonali, F.L., Corazzato, C., Tibaldi, A., 2011. Identifying rift zones on volcanoes: an example from La Réunion island, Indian Ocean. Bull. Volcanol. 73 (3), 347–366.

Brenna, M., Cronin, S.J., Németh, K., Smith, I.E.M., Sohn, Y.K., 2011. The influence of magma plumbing complexity on monogenetic eruptions, Jeju Island, Korea. Terra Nova 23 (2), 70–75.

Cardozo, N., Allmendinger, R.W., 2013. Spherical projections with OSXStereonet. Comput. Geosci. 51, 193–205.

Casas, A., Torné, M., Banda, E., 1986. Mapa gravimètric de Catalunya 1:500000. Servei Geològic de Catalunya. Dpt. De Política Territorial i Obres Públiques.

Catalan Geographic Institute (ICC). http://www.icc.cat/ (Accessed 15 January 2014).

Catalan Geologic Institute (IGC). http://www.igc.cat/ (Accessed 15 January 2014).

Cebrià, J.M., López-Ruiz, J., Doblas, M., Oyarzun, R., Hertogen, J., Benito, R., 2000. Geochemistry of the Quaternary alkali basalts of Garrotxa (NE Volcanic Province, Spain): a case of double enrichment of the mantle lithosphere. J. Volcanol. Geotherm. Res. 102, 217–235.

Cebrià, J.M., Martín-Escorza, C., López-Ruiz, J., Morán-Zenteno, D.J., Martiny, B.M., 2011. Numerical recognition of alignments in monogenetic volcanic areas: examples from the Michoacán–Guanajuato Volcanic Field in Mexico and Calatrava in Spain. J. Volcanol. Geotherm. Res. 201, 73–82.

Cimarelli, C., Di Traglia, F., Taddeucci, J., 2012. Basaltic scoria textures from a zoned conduit as precursors to violent Strombolian activity. Geology 38, 439–442.

Cimarelli, C., Di Tragia, F., de Rita, D., Gimeno Torrente, D., Fernandez Turiel, J.L., 2013. Space–time evolution of monogenetic volcanism in the mafic Garrotxa Volcanic Field (NE Iberian Peninsula). Bull. Volcanol. 75, 758.

Clemens, J.D., Mawer, C.K., 1992. Granitic magma transport by fracture propagation. Tectonophysics 204, 339–360.

Connor, C.B., Conway, F.M., 2000. Basaltic volcanic fields. In: Sigurdsson, H., Houghton, B.F., McNutt, S.R., Rymer, H., Stix, J. (Eds.), Encyclopedia of Volcanoes. Academic Press, San Diego, pp. 331–343.

Corazzato, C., Tibaldi, A., 2006. Fracture control on type, morphology and distribution of parasitic volcanic cones: an example from Mt. Etna, Italy. J. Volcanol. Geotherm. Res. 158 (1), 177–194.

Dèzes, P., Schmid, S.M., Ziegler, P.A., 2004. Evolution of the European Cenozoic Rift System: interaction of the Alpine and Pyrenean orogens with their foreland lithosphere. Tectonophysics 389, 1–33.

Di Maio, R., Mauriello, P., Patella, D., Petrillo, Z., Piscitelli, S., Siniscalchi, A., 1998. Electric and electromagnetic outline of the Mount Somma–Vesuvius structural setting. J. Volcanol. Geotherm. Res. 82, 219–238.

Di Maio, R., Patella, D., Petrillo, Z., Siniscalchi, A., Cecere, G., De Martino, P., 2000. Application of electric and electromagnetic methods to the definition of the Campi Flegrei caldera (Italy). Ann. Geofis. 43, 375–390.

Downes, H., 2001. Formation and modification of the shallow sub-continental lithospheric mantle: a review of geochemical evidence from ultramafic xenolith suites and tectonically emplaced ultramafic massifs of Western and Central Europe. J. Petrol. 42, 233–250.

Fernández, M., Torné, M., Zeyen, H., 1990. Lithospheric thermal structure of NE Spain and the North-Balearic basin. J. Geodyn. 12, 253–267.

Fiske, R.S., Jackson, E.D., 1972. Orientation and growth of Hawaiian volcanic rifts: the effect of regional structure and gravitational stresses. Proc. R. Soc. Lond. 329, 299–326.

Fontserè, E., Iglésies, J., 1971. Recopilació de dades sísmiques de les terres catalanes entre 1100 i 1906. Fundació Salvador Vives Casajuana, Barcelona, p. 548.

Galán, G., Oliveras, V., Paterson, B.A., 2008. Types of metasomatism in mantle xenoliths enclosed in Neogene–Quaternary alkaline mafic lavas from Catalonia (NE Spain). Geol. Soc. Lond. 293, 121–153.

Gallart, J., Olivera, C., Correig, A., 1984. Aproximación geofísica a la zona volcánica de Olot (Girona). Estudio local de sismicidad. Rev. Geofís. 40, 205–226.

Gallart, J., Pous, J., Boix, F., Hirn, A., 1991. Geophysical constraints on the structure of the Olot Volcanic Area, north-eastern Iberian Peninsula. J. Volcanol. Geotherm. Res. 47, 33–44.

Goula, X., Olivera, C., Fleta, J., Grellet, B., Lindo, R., Rivera, L.A., Cisternas, A., Carbon, D., 1999. Present and recent stress regime in the eastern part of the Pyrenees. Tectonophysics 308, 487–502.

Gretener, P.E., 1969. On the mechanics of the intrusion of sills. Can. J. Earth Sci. 6, 1415–1419.

Grosse, P., van Wyk de Vries, B., Petrinovic, I.A., Euillades, P.A., Alvarado, G., 2009. Morphometry and evolution of arc volcanoes. Geology 37, 651–654.

Grosse, P., van Wyk de Vries, B., Euillades, P.A., Kervyn, M., Petrinovic, I., 2012. Systematic morphometric characterization of volcanic edifices using digital elevation models. Geomorphology 136, 114–131. http://dx.doi.org/10.1016/j.geomorph.2011.06.001.

Gudmundsson, A., 2003. Surface stresses associated with arrested dykes in rift zones. Bull. Volcanol. 65, 606–619.

Gudmundsson, A., Philipp, S.L., 2006. How local stress fields prevent volcanic eruptions. J. Volcanol. Geotherm. Res. 158, 257–268.

Guérin, G., Behamoun, G., Mallarach, J.M., 1985. Un exemple de fusió parcial en medi continental. El vulcanisme quaternari de la Garrotxa 1. Publicació del Museu Comarcal de la Garrotxa, Vitrina, pp. 19–26.

Harangi, S., Sági, T., Seghedi, I., Ntaflos, T., 2013. Origin of basaltic magmas of Perşani volcanic field, Romania: a combined whole rock and mineral scale investigation. Lithos 180–181, 43–57.

IGME, 2011. Continuous Digital Geological Map of Spain, Canary Islands, 1:25.000, http://cuarzo.igme.es/sigeco/. Accessed 15 January 2014.

Jankovics, M.É., Dobosi, G., Embey-Isztin, A., Kiss, B., Sági, T., Harangi, S., Ntaflos, T., 2013. Origin and ascent history of unusually crystal-rich alkaline basaltic magmas from the western Pannonian Basin. Bull. Volcanol. 75, 1–23. http://dx.doi.org/10.1007/s00445-013-0749-7.

Karakhanian, A., Djrbashian, R., Trifonov, V., Philip, H., Arakelian, S., 2002. Holocene-historical volcanism and active faults as natural risk factors for Armenia and adjacent countries. J. Volcanol. Geotherm. Res. 113, 319–344.

Kavanagh, J.L., Menand, T., Sparks, R.S.J., 2006. An experimental investigation of sill formation and propagation in layered elastic media. Earth Planet. Sci. Lett. 245, 799–813.

Klugel, A., 1998. Reactions between mantle xenoliths and host magma beneath La Palma (Canary Islands): constraints on magma ascent rates and crustal reservoirs. Contrib. Mineral. Petrol. 131 (2), 237–257.

Kresic, N., 2010. Types and classifications of springs. In: Kresic, N., Stevanovic, Z. (Eds.), Groundwater Hydrology of Springs: Engineering, Theory, Management and Sustainability. Butterworth-Heinemann, p. 592.

Le Corvec, N., Menand, T., Lindsay, J., 2013. Spatial distribution and alignments of volcanic centers: clues to the formation of monogenetic volcanic fields. Earth Sci. Rev. 124, 96–114.

Llobera, P., 1983. Petrologia de los enclaves del volcán Roca Negra (Olot, NE España). Acta Geol. Hisp. 18, 19–25.

Martí, J., Mitjavila, J., Roca, E., Aparicio, A., 1992. Cenozoic magmatism of the Valencia trough (western Mediterranean): relationship between structural evolution and volcanism. Tectonophysics 203, 145–165.

Martí, J., Planagumà, L., Geyer, A., Canal, E., Pedrazzi, D., 2011. Complex interaction between Strombolian and phreatomagmatic eruptions in the Quaternary monogenetic volcanism of the Catalan Volcanic Zone (NE of Spain). J. Volcanol. Geotherm. Res. 201, 178–193.

Martí, J., Pinel, V., López, C., Geyer, A., Abella, R., Tárraga, M., Blanco, M.J., Castro, A., Rodríguez, C., 2013. Causes and mechanisms of the 2011–2012 El Hierro (Canary Islands) submarine eruption. J. Geophys. Res. Solid Earth 118, 823–839. http://dx.doi.org/10.1002/jgrb.50087.

Mattsson, H.B., 2012. Rapid magma ascent and short eruption durations in the Lake Natron–Engaruka monogenetic volcanic field (Tanzania): a case study of the olivine melilititic Pello Hill scoria cone. J. Volcanol. Geotherm. Res. 247–248, 16–25.

McGee, L., Beier, C., Smith, I., Turner, S., 2011. Dynamics of melting beneath a small-scale basaltic system: a U-Th–Ra study from Rangitoto volcano, Auckland volcanic field, New Zealand. Contrib. Mineral. Petrol. 1–17.

Michon, L., Merle, O., 2005. Discussion on "Evolution of the European Cenozoic Rift System: interaction of the Alpine and Pyrenean orogens with their foreland lithosphere". Tectonophysics 401, 251–256.

Moreno, V., Bach, J., Baixeras, C., Font, L., 2014. Radon levels in groundwaters and natural radioactivity in soils of the volcanic region of La Garrotxa, Spain. J. Environ. Radioact. 128, 1–8.

Neumann, E.R., Martí, J., Mitjavila, J., Wulff-Pedersen, E., 1999. Origin and implications of marie xenoliths associated with Cenozoic extension-related volcanism in the Valencia Trough, NE Spain. Mineral. Petrol. 65, 113–139.

Nishi, Y., Ishido, T., Matsushima, N., Ogawa, Y., Tosha, T., Myazaki, J., Yasuda, A., Scott, B.J., Sherbum, S., Bromley, C., 1996. Self-potential and audio-magnetotelluric survey in White Island Volcano. New Zealand Geothermal Workshop (http://www.geothermal-energy.org/pdf/IGAstandard/NZGW/1996/Nishi.pdf).

Olivera, C., Fleta, J., Susagna, T., Figueras, S., Goula, X., Roca, A., 2003. Seismicity and recent deformations in the northeastern of the Iberian Peninsula. Fís. Tierra 15, 111–114.

Olivera, C., Redondo, E., Lambert, J., Riera Melis, A., Roca, A., 2006. Els terratrèmols dels segles XIV i XV a Catalunya. Monografies 30. Institut Cartogràfic de Catalunya, Barcelona, p. 407.

Paulsen, T.S., Wilson, T.J., 2010. New criteria for systematic mapping and reliability assessment of monogenetic volcanic vent alignments and elongate volcanic vents for crustal stress analyses. Tectonophysics 482, 16–28.
Perea, H., 2009. The Catalan seismic crisis (1427 and 1428; NE Iberian Peninsula): geological sources and earthquake triggering. J. Geodyn. 47, 259–270.
Portal, A., Labazuy, P., Lénat, J.F., Béné, S., Boivin, P., Busato, E., Cârloganu, C., Combaret, C., Dupieux, P., Fehr, F., Gay, P., Laktineh, I., Miallier, D., Mirabito, L., Niess, V., Vulpescu, B., 2013. Inner structure of the Puy de Dôme volcano: cross-comparison of geophysical models (ERT, gravimetry, muon imaging). Geosci. Instrum. Methods Data Syst. 2, 47–54 (Revil A (2002)).
Rubin, A.M., 1995. Propagation of magma-filled cracks. Annu. Rev. Earth Planet. Sci. 23, 287–336.
Sachs, P.M., Stange, S., 1993. Fast assimilation of xenoliths in mag-mas. J. Geophys. Res. 98 (B11), 19741–19754.
Saula, E., Picart, J., Mató, E., Llenas, M., Losantos, M., Berasategui, X., Agustí, J., 1996. Evolución geodinámica de la fosa del Empordà y de las Sierras Transversales. Acta Geol. Hisp. 29, 55–75.
Sparks, R.S.J., Pinkerton, H., Macdonald, R., 1977. The transport of xenoliths in magmas. Earth Planet. Sci. Lett. 35 (2), 234–238.
Sparks, R.S.J., Baker, L., Brown, R.J., Field, M., Schumacher, J., Stripp, G., Walters, A., 2006. Dynamical constraints on kimberlite volcanism. J. Volcanol. Geotherm. Res. 155 (1–2), 18–48.
Spera, F.J., 1980. Aspects of magma transport. In: Hargraves, R.B. (Ed.), Physics of magmatic processes. Princeton University Press, pp. 265–323.
Spera, F.J., 1984. Carbon dioxide in petrogenesis III: role of volatiles in the ascent of alkaline magma with special reference to xenolith-bearing mafic lavas. Contrib. Mineral. Petrol. 88, 217–232.
Szabó, C., Bodnar, R.J., 1996. Changing magma ascent rates in the Nógrád–Gömör volcanic field, Northern Hungary/Southern Slovakia: evidence from CO2-rich fluid inclusions in metasomatized upper mantle xenoliths. Petrology 4 (3), 221–230.
Tibaldi, A., 1995. Morphology of pyroclastic cones and tectonics. J. Geophys. Res. Solid Earth 100 (B12), 24521–24535.
Tibaldi, A., 2003. Influence of cone morphology on dykes, Stromboli, Italy. J. Volcanol. Geotherm. Res. 126, 79–95.
Tibaldi, A., Bonali, F.L., Corazzato, C., 2014. The diverging volcanic rift system. Tectonophysics 611, 94–113.
Tsuchiyama, A., 1986. Melting and dissolution kinetics: application to partial melting and dissolution of xenoliths. J. Geophys. Res. 91 (B9), 9395–9406.
Vona, A., Romano, C., Dingwell, D.B., Giordano, D., 2011. The rheology of crystal-bearing basaltic magmas from Stromboli and Etna. Geochim. Cosmochim. Acta 75, 3214–3236.
Walker, G.P.L., 1999. Volcanic rift zones and their intrusion swarms. J. Volcanol. Geotherm. Res. 94, 21–34.
Wattananikorn, K., Kanaree, M., Wiboolsake, S., 1998. Soil gas radon as an earthquake precursor: some considerations on data improvement. Radiat. Meas. 29, 593–598.
Zarroca, M., Linares, R., Bach, J., Roqué, C., Moreno, V., Font, L., Baixeras, C., 2012. Integrated geophysics and soil gas profiles as a tool to characterize active faults: the Amer fault example (Pyrenees, NE Spain). Environ. Earth Sci. 67, 889–910.
Zeyen, H.J., Banda, E., 1988. Geophysical mapping in Catalonia. Aeromagnetic map. Rev. Soc. Geol. Esp. 1 (1–2), 73–79.
Ziegler, P.A., 1992. European Cenozoic rift system. In: Ziegler, P.A. (Ed.), Geodynamics of Rifting, Volume I. Case History Studies on Rift: Europe and Asia. Tectonophysics 208, pp. 91–111.